Steel and Composite Structures, *Vol. 22, No. 4 (2016) 837-853*
DOI: http://dx.doi.org/10.12989/scs.2016.22.4.837

Residual stress of cold-formed thick-walled steel rectangular hollow sections

Xingzhao Zhang [1], Su Liu [1], Mingshan Zhao [*2], and Sing-Ping Chiew [3]

[1] *School of Architecture, Hunan University, P.R. China*
[2] *School of Civil and Environmental Engineering, Nanyang Technological University, Singapore*
[3] *Singapore Institute of Technology, Singapore*

(*Received September 19, 2015, Revised October 18, 2016, Accepted October 31, 2016*)

Abstract. This paper presents the experimental and numerical study on the distribution of transverse and longitudinal residual stresses in cold-formed thick-walled structural steel rectangular hollow sections manufactured by indirect technique. Hole-drilling method is employed to measure the magnitude of the transverse and longitudinal surface residual stress distribution, and the effects of the residual stresses are evaluated qualitatively by sectioning method. It is shown that compared to normal cold-formed thin-walled structural hollow sections (SHS), the cold-formed thick-walled SHS has similar level of residual stress in the flat area but higher residual stresses in the corner and welding areas. Both the transverse and longitudinal residual stresses tend to open the section. In order to predict the surface residual stresses in the corners of the cold-formed thick-walled SHS, an analytical model is developed. 2D finite element simulation of the cold bending process is conducted to validate the analytical approach. It is shown that in analyzing bending for thick-walled sections, shifting of neutral axis must be considered, since it would lead to non-linear and non-symmetrical distribution of stresses through the thickness. This phenomenon leads to the fact that cold-formed thick-walled SHSs has different distribution and magnitude of the residual stresses from the cold-formed thin-walled SHSs.

Keywords: cold-formed; thick-walled; structural hollow section; residual stress; analytical model

1. Introduction

Cold-formed steel structural hollow sections (SHS) are widely used as load-bearing members in welded frame structures. In early stage, common rectangular hollow sections could only be fabricated as thin-walled sections with thickness ranging from 0.4 to 6 mm (Tong *et al*. 2012). For sections with increased thickness, it was difficult to control the through thickness properties at the cold-forming zones. Theoretically speaking, thin-walled or thick-walled, cold-formed SHSs (referring to rectangular hollow sections in this paper) are formed by rolling an annealed flat strip by direct or indirect methods. The direct method bends the strip into the final SHS shape directly, while the indirect method rolls the flat strip into circular hollow section first and further rolls it into the rectangular shape (Gardener *et al*. 2010). The manufacturing processes usually do not include post-forming stress relief. As a result, there remains complex distributions of yield strength and residual stress around the section (Key and Hancock 1993). The existence of residual stresses

*Corresponding author, Ph.D., E-mail: mszhao@ntu.edu.sg

http://www.techno-press.org/?journal=scs&subpage=6 ISSN: 1229-9367 (Print), 1598-6233 (Online)

is mainly due to strain hardening, welding, flame cutting and heat treatment (Abambres and Quach 2016). Through decades of study and practice, the importance of residual stress for designing and analyzing steel structures has been well recognized, as it is frequently associated with issues such as brittle fracture, fatigue, stress corrosion, buckling and post-buckling strength reduction (Wang *et al*. 2012, Ma *et al*. 2015). Common design standards have taken the effect of residual stresses into consideration implicitly (AISC 2005, BSI 2005). However, there are few specific guidelines on designing and evaluating the distribution of the residual stress directly.

Since the residual stress distribution in cold-formed sections are complex and highly dependent on the forming techniques, material properties and section profile, experimental approach is more frequently adopted than theoretical approach in the investigation (Withers *et al*. 2008). For residual stress contained in cold-formed thin-walled SHSs, numerous work has been done (Moen *et al*. 2008, Spoorenberg *et al*. 2010, Jandera and Machacek 2014). It is well recognized that the longitudinal residual stresses are in tension at outer surface and in compression at inner surface, and the distribution is assumed to be linear through the thickness (Mashiri *et al*. 2014). However, studies on the cold-formed thick-walled plate subjected to bending (Weng and White 1990, Key and Hancock 1993) show that the through thickness residual stress distribution pattern is non-linear. Tong *et al*. (2012) measured the longitudinal residual stress distribution of a few thick-walled cold-formed SHSs and found out the magnitude of the residual stress at the corner was lower than that at flat area, which is also different from the common cold-formed thin-walled SHSs. Up to date, the literature on the residual stress distribution in cold-formed thick-walled SHSs is still limited, especially for residual stresses in the transverse direction (Li *et al*. 2009, Gardener *et al*. 2010, Ma *et al*. 2015).

The main objective of this study is to investigate the distribution of transverse and longitudinal residual stresses contained in cold-formed thick-walled SHSs by both experimental and numerical methods. In the experimental investigation, the geometrical and mechanical properties of the selected cold-formed thick-walled SHS are firstly obtained. Subsequently, the hole-drilling technique is used to quantitatively measure the magnitude of residual stresses on the outer surface in both transverse and longitudinal directions. Further, the effect of the locked-in residual stress is qualitatively evaluated by the sectioning method. Comparison between the experimental findings and existing literature is also presented. In the second phase, numerical investigation is conducted. An analytical elastic-plastic large displacement model is developed to predict the surface residual stress distribution in the corner. 2D finite element (FE) is also employed to simulate the forming of residual stress in the same area. By comparing the strain and stress distributions in bending and the following springback stage of these two models, the proposed analytical model is validated.

2. Experimental investigation

2.1 Geometrical dimensions

As shown in Fig. 1, the following characteristic dimensions are measured for the tested SHS: width b and wall thickness t of every face, inner corner radii (r_i) and outer corner radii (r_o) of four corners. Based on the mean values of the above dimensions, the main geometrical parameters including wall slenderness ratio b_m/t_m, mean center corner radii $r_{c,m}$, mean outer corner radii related to mean wall thickness $r_{o,m}/t_m$ and mean center corner radii related to mean wall thickness $r_{c,m}/t_m$ are calculated, as shown in Table 1. Theoretically, the differences between thin-walled and thick

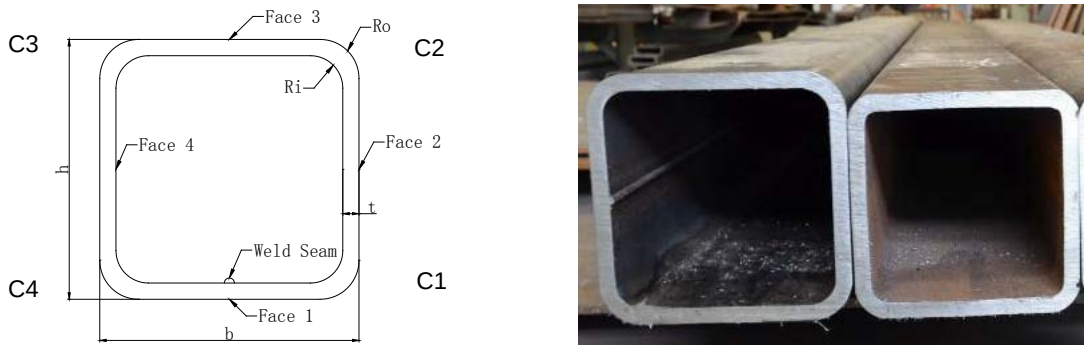

(a) Definition of the measured geometrical dimensions

(b) The tested cold-formed SHS (left) in comparison with a hot-formed SHS (right)

Fig. 1 Definition of the measured geometrical dimensions and the tested SHS

Table 1 Characteristic geometrical dimensions of the tested SHS

Hollow sections	b_m (mm)	t_m (mm)	$r_{o,m}$ (mm)	$r_{i,m}$ (mm)	b_m/t_m	$r_{o,m}/t_m$	$r_{c,m}/t_m$
Cold-formed	200.53	12.76	31.00	18.75	15.72	2.43	2.49
EN 10219	200±1.6	12.5±0.5				2.4 to 3.6	

walled SHSs come from the rolling process only. There is no strict criterion for determining whether a cold-formed SHS is thin-walled or thick-walled. For common cold-formed SHSs, the center corner radius over thickness ratio (r_c/t) is restricted to be within 2 to 6 (AISI 1996). Any section with r_c/t close to 2 would behave like the thick-walled, while that with r_c/t close to 6 would behave similar to the thin-walled.

2.2 Mechanical properties

Standard coupon specimens are cut from the center areas of Faces 2, 3 and 4 (Fig. 2) and tested according to EN 10002-1 (BSI 2001). The dimensions of the specimens are shown in Fig. 2. Non-proportional gauge length of 80mm is used as the original gauge length. For conversion of elongation values from non-proportional gauge length to a proportional gauge length $5.65\sqrt{S_o}$, the conversion tables from BS EN 2566-1 (BSI 1999) is applied. During tests, both strain gauge and extensometer are used for stress-strain relationship measurement. The loading rate is set as 1 mm/min and stress-strain data points are captured at frequency of 1 Hz.

The stress-strain curves of the tested coupon specimens are shown in Fig. 3 in comparison with a typical curve of hot-formed S355J2H. The characteristic mechanical properties of all the tested specimens are shown in Table 2, in comparison with the requirements by the corresponding product standard EN 10219 (BSI 2006). It can be seen from Fig. 3 and Table 2 that the mechanical properties of the cold-formed and hot-formed SHSs differ remarkably, although they consist of similar contents of elements. Firstly, the cold-formed SHS literally fulfills the mechanical property specifications of S460NH. Due to the strain hardening by cold forming, the average yield strength of the cold-formed SHS is 27.1% higher than that of the hot-formed SHS. However, this improvement in strength is obtained at the expense of ductility. The cold-formed SHS does not

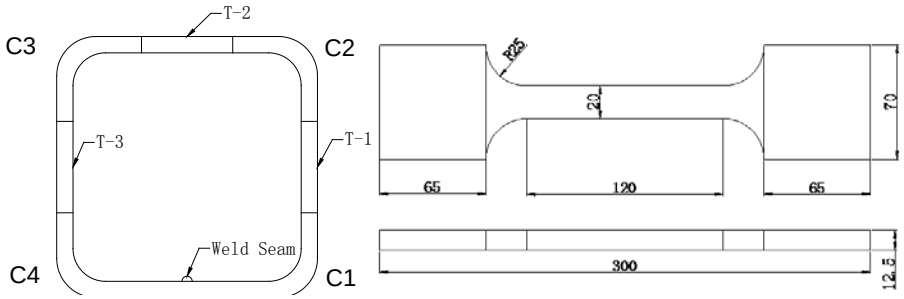

Fig. 2 Sources and dimensions of tensile test specimens

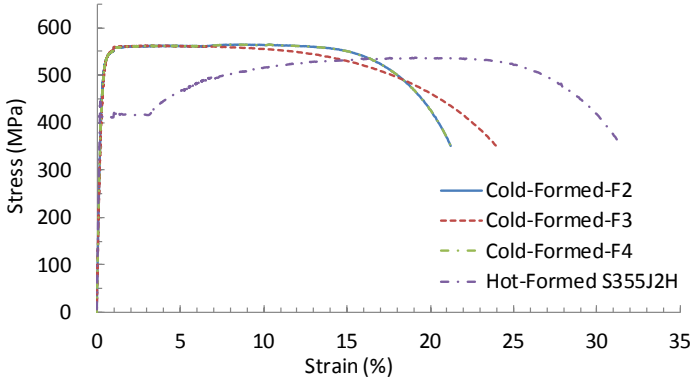

Fig. 3 Stress-strain curves of the tested SHS

Table 2 Summary of the tensile test results

SHS	f_y (MPa)	Ave. (MPa)	f_u (MPa)	Ave. (MPa)	E (GPa)	Ave. (GPa)	Tensile ratio	Ave.	Elongation (%)
Cold-formed	529.3	521.1	562.2	559.2	208.3	208.4	1.06	1.07	21.5
	511.0		551.6		209.2		1.08		23.6
	523.0		563.7		207.7		1.08		21.8
EN 10219 S460NH	≥ 460		≥ 540 ≤ 720						≥17
Hot-formed	410.6		531.0		208.7		1.29		31

show obvious yield plateau and both tensile ratio and elongation at fracture of the cold-formed SHS is remarkably lower than the hot-formed SHS.

2.3 Residual stress

2.3.1 Test method

In this study, the hole-drilling method is employed to quantitatively measure the residual stresses along the perimeter of the SHS. RS200 milling guide and electric strain gauge FRAS-2-11 are employed to measure the residual stresses released by hole drilling. Test positions are arranged

with equal distance on all the surfaces, and extra test points are added at corners and welding areas. The arrangement of the drilling points on the SHS is shown in Fig. 4(a). During the test, a hole with diameter of 2 mm and depth of 2 mm is drilled at the designated position on the special strain gauge rosette by 8 steps. The released strains at the end of each step are recorded for further analyzing. By comparing the strains before and after hole-drilling, stress relaxation due to hole drilling can be determined. On the assumptions that the material is homogeneous and isotropic and the stress-strain curve is linear, the relieved strain at the tested point can be obtained by substituting the stress relaxation into the Hooke's Law (ASTM 2008)

$$\varepsilon = \frac{1+v}{E}\bar{a}\frac{\sigma_{\emptyset}+\sigma_{\theta}}{2} + \frac{1}{E}\bar{b}\frac{\sigma_{\emptyset}-\sigma_{\theta}}{2}\cos 2\alpha + \frac{1}{E}\bar{b}\tau_{\emptyset\theta}\sin 2\alpha \tag{1}$$

In Eq. (1), E is the Young's modulus, v is the Poisson's ratio and ε is the relieved strain. $\sigma_{\emptyset}$ and σ_{θ} are the stresses in the $\emptyset$ and θ directions (Fig. 4(b)), respectively. α is the angle from the x-axis to the maximum principle stress, and $\bar{a}$ and $\bar{b}$ are almost material-independent calibration constants indicating the relieved strains due to unit stresses within the hole depth. Since the holes are drilled directly on the surface of the tubes (Fig. 4(b)) and the stress/strain status of the SHS can be treated as plane strain condition, $\sigma_{\emptyset}$ and σ_{θ} correspond to the transverse and longitudinal stresses. It should also be noted that the relieved strains are mostly influenced by the near-surface residual stresses. Interior stresses have influences that diminish with their depth from the surface (ASTM 2008). For the strain rosettes employed in this study (Fig. 4(b)), the sensitivity diminishes to near zero for stresses beyond 1mm depth. Therefore, the measurement actually indicates a weighted average of the residual stresses within the near-surface layer, i.e., 1 mm deep from the measured surface. Besides, the surface strains that will be relieved by drilling a hole depend only on the stresses that originally existed at the boundaries of the hole. The stresses beyond the hole boundary do not affect the relieved strains, even though the strains are measured beyond the hole boundary. In this study, the outer radius, 31.0 mm, is relatively large compared to the hole size. Therefore, it is assumed that Eq. (1) is still valid for the corners.

Besides the hole-drilling method, the sectioning test is also employed to evaluate the effect of the residual stresses. The sectioning test is carried out on SHS specimens with length of 200 mm. Three cuts with equal spacing and depth (170 mm) are applied on the flat area of each face, as shown in Fig. 5. By measuring the changes in the geometry before/after sectioning, the effects of the locked-in residual stress are evaluated.

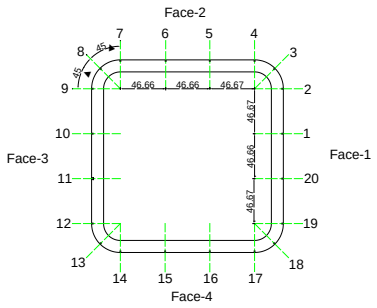

(a) Test positions

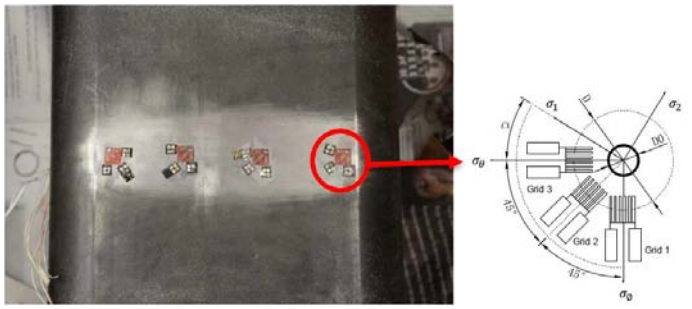

(b) Strain gauge rosette and coordinate system of stresses

Fig. 4 Hole drilling test

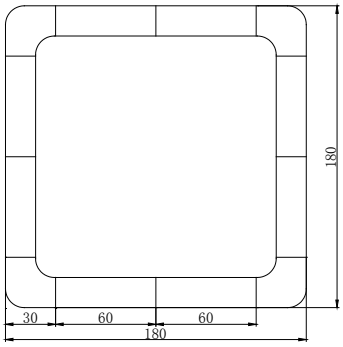

(a) Cutting positions

(b) Sectioning in progress

Fig. 5 Sectioning test

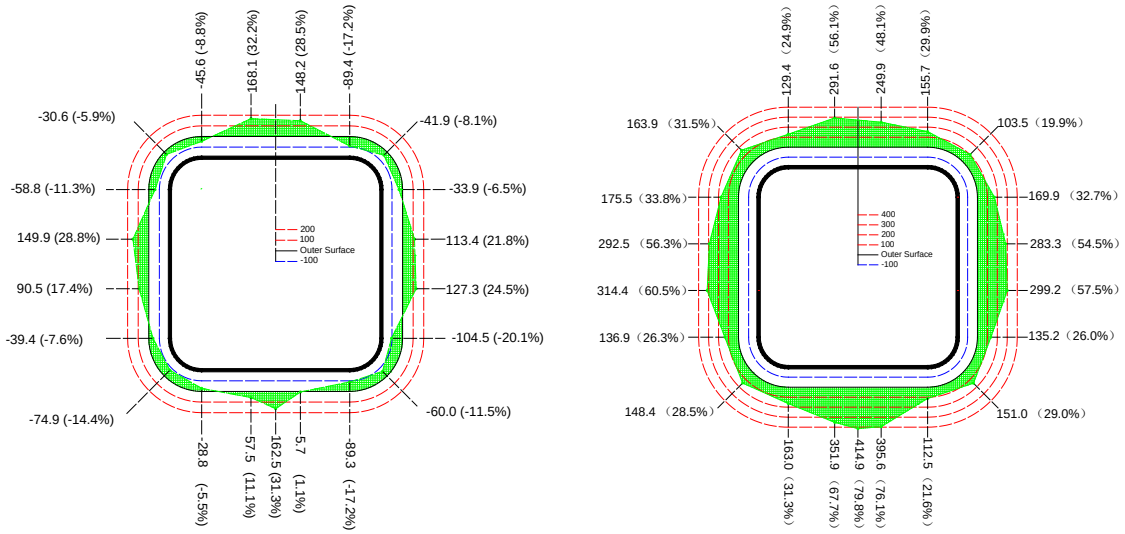

(a) Residual stress in the transverse direction

(b) Residual stress in the longitudinal direction

Fig. 6 Residual stress distribution (MPa and %) of the cold-formed SHS

2.3.2 Test results

The residual stress distributions in both transverse and longitudinal directions of the cold-formed SHS are shown in Fig. 6. The results for the flat area, corner and welding zone are also summarized in Table 3. In the above figures and tables, residual stresses are evaluated using both absolute value (MPa) and percentage over the yield strength (residual stress/actual yield strength × 100%). It can be seen from Fig. 6 that the distributions of the residual stress in both directions are generally symmetrical about the neutral axes.

In the transverse direction, the residual stresses are compressive stresses at the corners and tensile stresses elsewhere. The residual stress levels of the corner range from -20.1% to -5.9%; those of the flat area range from 17.4 to 32.2%; while those of the welding zone range from 1.1% to 31.3%. On the general level, the stress level is relatively low. Only 2 out of 21 positions show residual stress level higher than 30%. Based on the weighted average stresses in different zones,

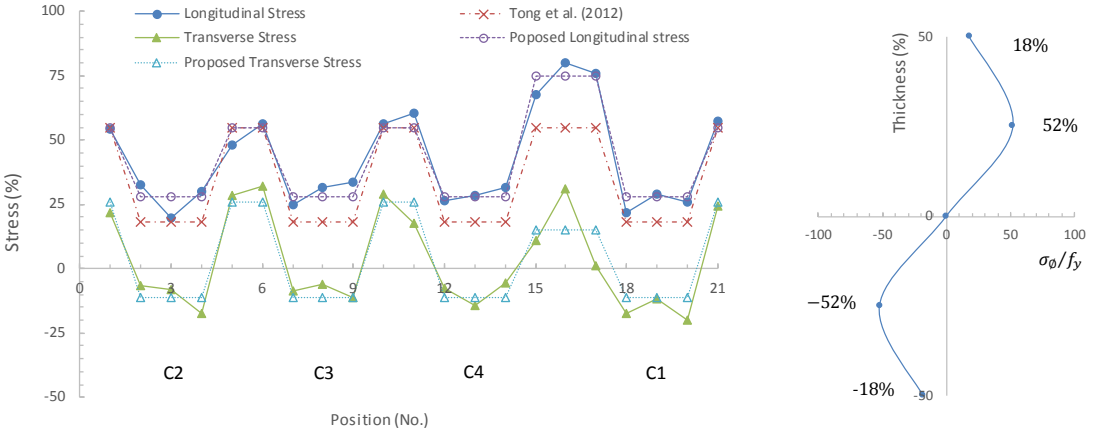

(a) Surface residual stress distribution

(b) Through thickness stress distribution (Tong *et al*. 2012)

Fig. 7 Residual stress distribution (%) of the cold-formed SHS

a prediction model is proposed, as shown in Fig. 7(a) and Table 3. To maintain the stress equilibrium through the thickness, it is obvious that the residual stresses at the inner surface of the SHS would be tensile stresses at the corners and compressive stresses elsewhere. It is predictable that this distribution would tend to open the section.

In the longitudinal direction, the residual stresses are all tensile stresses and the stress level is generally higher than the level of transverse residual stresses. It can be seen from Table 3 that the residual stress levels of the corner vary from 19.9% to 32.8% while most of the rest areas have residual stress level higher than 50%. Further, the longitudinal residual stress distribution is compared with the surface longitudinal residual stress model for indirectly cold-formed SHS proposed by Tong *et al*. (2012), as shown in Fig. 7. Tong *et al*. (2012) suggested values of 55% and 18% for the surface longitudinal stresses for the corner and flat area, respectively, and a symmetrical through thickness distribution (Fig. 7(b)). From the comparison (Fig. 7(a)), it is shown that this prediction model agrees well with the test results for the flat area, but is too low for the corner and welding zone. The possible deduction is that the model proposed by Tong *et al*. (2012) underestimates the stress level for thick-walled cold-forming processes and the residual stress induced by highly localized welding heat input. In fact, the residual stress caused by welding should be much higher than the flat area, and the assumption of symmetrical stress distribution in the thickness direction (Fig. 7(b)) is no longer accurate for thick-walled cold formed members. Herein, a new model is proposed for the distribution of surface longitudinal residual stresses in thick-walled cold-formed SHS. Special caution is given to the welding zone and corner area, as shown in Fig. 7(a) and Table 3.

Fig. 8(a) shows the specimen before and after sectioning. It can be seen from Fig. 8(a) that the section opens after sectioning and the section width increases by 4.5%. Both the through thickness transverse and longitudinal residual stresses contribute to this phenomenon through the membrane and bending actions (Gardener *et al*. 2010). While the transverse residual stresses are more prone to open the section (Fig. 6(a)), the longitudinal residual stresses are more likely to bend the section wall. As shown in Fig. 8b, these 300mm long and 70mm wide coupons cut from the flat area show convexity of about 1% after cutting.

Table 3 Residual stress in the transverse direction

	Flat area (%)	Proposed (%)	Corner (%)	Proposed (%)	Welding zone (%)	Proposed (%)
Transverse	17.4% to 32.2%	26%	-20.1 to -5.9%	-11%	1.1% to 31.3%	15%
Longitudinal	48.1% to 60.5%	55%	19.9% to 33.8%	28%	67.7% to 79.8%	75%

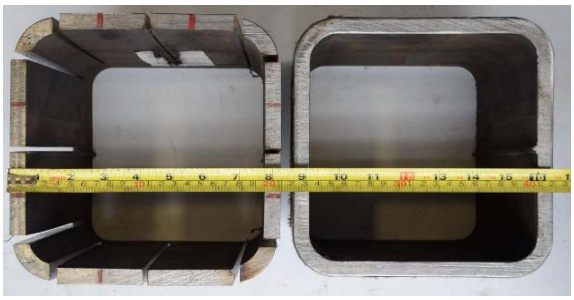

(a) Sectioning test

(a) Coupons bent due to residual stresses

Fig. 8 Sectioning test results of the cold-formed thick-walled SHS

3. Analytical model for residual stress induced by cold bending

3.1 Theory of residual stress formed during bending

Despite that there are many technologies to form a structural SHS, the residual stresses are always the result of mechanical and thermal actions. For cold-formed SHS, residual stresses can be induced by (1) cold bending; (2) welding; and (3) flame cutting (Ma *et al*. 2015). Since the welding and flame cutting only affect the material locally, this study focus on the residual stress formed by cold bending only. Fig. 9 shows a typical roll-forming process for the corners of rectangular SHSs. During bending, the material between the roller die reactions is expected to undergo certain level of yielding as the stress distribution transits from elastic to plastic. After the plate becomes fully plastic, the engineering strain continues to increase as the rolling radius keeps increasing. When the final bending radius is reached and the imposed radial displacement is removed, an elastic springback occurs and unload the corner. At the meantime, certain level of stress is locked-in as residual stress (Moen *et al*. 2008). It should be pointed out that in the above processes, the distribution of residual stress is dependent only on the geometry and mechanical properties including the yield strength/tensile strength and elastic/plastic modulus (Liu *et al*. 2015). Compared to the cold-formed SHS, the hot-formed SHSs are less concerned regarding the residual stress because the hot-formed SHSs are rolled at high temperature conditions where both the strengths and elastic/plastic modulus are significantly lower than at room temperature.

In this study, a general analytical model for predicting the surface residual stresses in the corners of the cold-formed thick-walled SHSs is proposed. In the case of thick-walled (small radius) bending, many commonly used beam analysis assumptions are no longer valid such as the symmetrical through thickness stress distribution assumption, middle surface neutral axis assumption and engineering strain method (Amouzegar *et al*. 2016). Therefore, a series of analytical assumptions must be defined first.

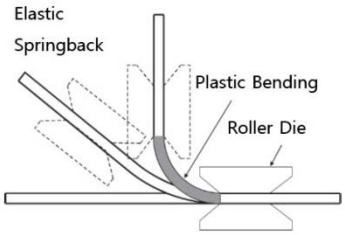

Fig. 9 Roll-forming for corners of SHS

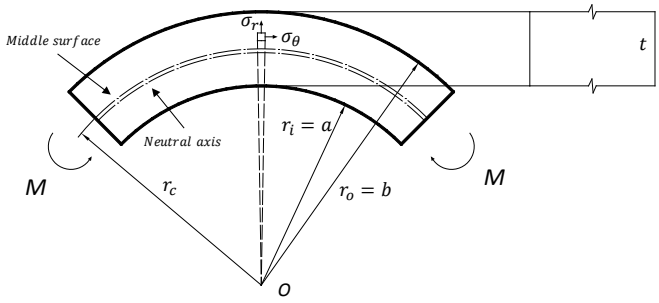

Fig. 10 Stress-strain coordinate system

3.2 Assumptions for the analytical model

The stress-strain coordinate system is shown in Fig. 10. Based on this system, the following assumptions are established.

(1) This problem is simplified as plane strain problem and the thickness of the section remain the unchanged throughout the process. On the inner and outer surfaces, the following boundary conditions apply: for $r = r_i$ and $r = r_o$, $\sigma_r = 0$. For further simplification, the through thickness stresses in the radial direction are all neglected, i.e., $\sigma_r = 0$ for $r_i < r < r_o$. This assumption avoids the tri-axial stress status analysis, since the radial stress is only significant near the neutral axis. This approach is widely adopted in the measurement of residual stresses by techniques such as hole drilling and sectioning methods (Ma *et al*. 2015).

(2) Logarithmic stress-strain (true stress-strain) relationship is adopted in the analysis, since large deformation is involved. As indicated by Yu and Zhang (Yu and Zhang 1996), for pure bending of wide plates with center line bending radius $r_c \leq 10\,t$, the adopting of true stress-strain is necessary.

(3) The neutral axis remains unchanged during cross-section bending. For large curvature bending analysis, the neutral axis no longer coincides with the middle surface. It is slightly shifted to the inner surface side and the distance would further increase when plasticity takes place (Zhu 2007). In this study, only the initial position of the neutral axis is calculated and the second shift caused by plasticity is ignored to simplify the derivation.

(4) This approach only predicts the residual stresses formed by cold-bending, which are between the roller die reactions (Fig. 9). In reality, some yielding is expected to occur outside the roller reactions as the stress distribution transits from fully plastic to fully elastic, and the stress distribution may not be uniform throughout the corners.

3.3 Residual stress from cross-section bending

It is common to use simplified stress-strain curves such as linear elastic-perfectly plastic and elastic-plastic with linear strain hardening in theoretical study, as shown in Fig. 11(a). The following effective stress ($\bar{\sigma}$) and effective strain ($\bar{\varepsilon}$) relationship is firstly established:

$$\bar{\sigma} = f_y + E_p\left(\bar{\varepsilon} - \varepsilon_y\right) = \left(E - E_p\right)\varepsilon_y + E_p\,\bar{\varepsilon} \tag{2}$$

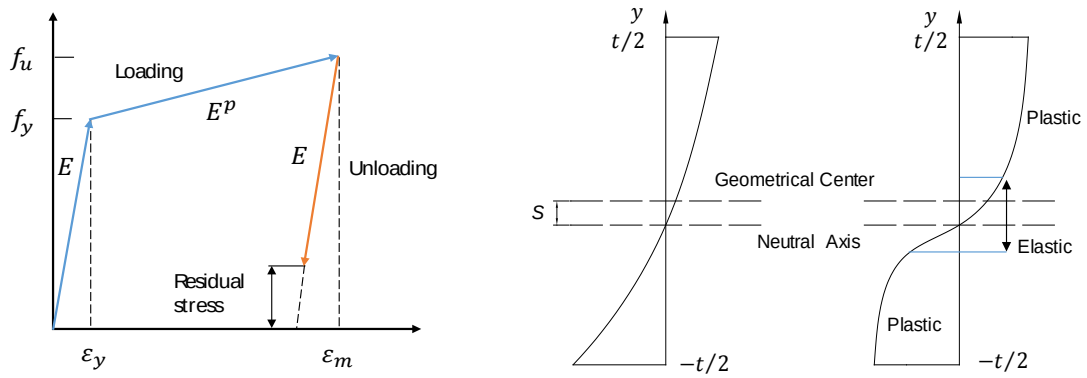

(a) Stress-strain model (b) Transverse stress

Fig. 11 Stress-strain behavior during bending

where f_y and ε_y are the true stress and strain at yielding, respectively. E and E_p are the elastic and plastic modulus, respectively. Based on the engineering stress-strain curves (Fig. 3), the true stress-strain relationship is obtained: $f_y = 521.1$ MPa, $\varepsilon_y = 0.00251$ and $E_p = 585.1$ MPa.

Under the situation of pure bending for curved beam system (Fig. 10), there are two possible patterns of stress/strain distribution over the cross-section, as shown in Fig. 11(b).

(a) When the cross section is not yet yielded, the non-linear stress distribution can be expressed by (Timoshenko and Goodier 1970)

$$\sigma_\theta = -\frac{4M}{N}\left(-\frac{a^2b^2}{r^2}log\frac{b}{a} + b^2 log\frac{r}{b} + a^2 log\frac{a}{r} + b^2 - a^2\right) \tag{3a}$$

$$\sigma_r = -\frac{4M}{N}\left(\frac{a^2b^2}{r^2}log\frac{b}{a} + b^2 log\frac{r}{b} + a^2 log\frac{a}{r}\right) \tag{3b}$$

$$\tau_{r\theta} = 0 \tag{3c}$$

where $N = (b^2 - a^2)^2 - 4a^2b^2(log\frac{b}{a})^2$ is a constant. As stated previously, the σ_r is only significant near the neutral axis and equals to zero on the surface. Therefore, it is neglected in this study. By substituting geometrical data into (3a), the neutral axis position (shift from middle surface by s) can be easily determined by solving $\sigma_\theta(r) = 0$. Besides, since $\tau_{r\theta} = 0$, σ_θ and σ_r become principal stresses in the bending plane (Fig. 10) naturally.

(b) When the outer and inner surfaces are yielded while the core remains elastic, an arbitrary point in the sheet undergoes transverse straining with the amount depending on its location y away from the current neutral axis (Fig. 11(b)). By the assumption of $\sigma_\theta = 0$ at the neutral axis, the true transverse strain due to cold bending can be obtained (Quach *et al.* 2004)

$$\varepsilon_\theta = \ln\left[1 + \left(\frac{s - y}{r_c - s}\right)\right] \tag{4}$$

For the elastic core, the transverse and longitudinal stresses are governed by Hooke's Law. Due to assumption (1) made in section 3.2, the stress and strain in the through thickness direction are ignored, i.e., $\sigma_r = 0$ and $\varepsilon_r = 0$. The stress-strain state can be expressed as

$$\sigma_\theta = \frac{E}{1-v^2}(\varepsilon_\theta + v\varepsilon_\emptyset) = \frac{E}{1-v^2}\varepsilon_\theta \tag{5a}$$

$$\sigma_\emptyset = v\sigma_\theta = \frac{vE}{1-v^2}\varepsilon_\theta \tag{5b}$$

For the point just reaches yielding, the stress state is governed by Von Mises principle

$$\bar{\sigma} = \sqrt{\sigma_\theta^2 + \sigma_\emptyset^2 - \sigma_\theta\sigma_\emptyset} \tag{6}$$

By substituting Eqs. (5a) and (5b) into (6)

$$\varepsilon_\theta = \pm\bar{\sigma}(1-v^2)/(E\sqrt{1-v+v^2}) \tag{7}$$

where $\varepsilon_\theta > 0$ if the strain is tensile ($y > s$) and $\varepsilon_\theta < 0$ if the strain is compressive ($y < s$). Together with Eq. (4), the range of the elastic zone can be defined

$$s-(r_c-\mathrm{s})(\mathrm{e}^{\frac{\bar{\sigma}(1-v^2)}{E\sqrt{1-v+v^2}}}-1) \le y \le s-(r_c-\mathrm{s})(\mathrm{e}^{\frac{-\bar{\sigma}(1-v^2)}{E\sqrt{1-v+v^2}}}-1) \tag{8}$$

For the plastic zone, the stresses are subjected to plastic straining. The following stress ratio can be defined

$$\sigma_\emptyset = \omega\sigma_\theta \tag{9}$$

where $\omega = 0.5$ is adopted in this analysis (Massonnet *et al*. 1979). Combining Eqs. (6) and (9), the stress of any point undergoing plastic straining due to cold bending can be expressed as

$$\sigma_\theta = \pm\frac{\bar{\sigma}}{\sqrt{1-\omega+\omega^2}} \tag{10a}$$

$$\sigma_\emptyset = \pm\frac{\omega\bar{\sigma}}{\sqrt{1-\omega+\omega^2}} \tag{10b}$$

where σ_θ and $\sigma_\emptyset > 0$ when $y > s$; and σ_θ and $\sigma_\emptyset < 0$ when $y < s$.

For the equivalent plastic strain, the following relationships exist

$$\overline{\varepsilon^p} = \sqrt{\varepsilon_\theta^2 + \varepsilon_\emptyset^2 - \varepsilon_\theta\varepsilon_\emptyset} = \frac{\sqrt{3}}{2}\varepsilon_\theta \tag{11a}$$

$$\bar{\varepsilon} = \varepsilon^p + \frac{\bar{\sigma}}{E} \tag{11b}$$

With the true stress-strain relationship governed by Eq. (2), the through thickness distribution

of σ_θ and $\sigma_\emptyset$ can be solved by Eqs. (10) and (11), while the bending moment is calculated as

$$M_{bend} = \int_{-t/2}^{t/2} \sigma_\theta y dy \tag{12}$$

When the final bending radius is reached and the imposed radial displacement is removed, an elastic springback would occur and elastically unload the corner (Fig. 9). To simulate the elastic rebound of the bending process, this plastic moment is applied elastically through the thickness by using Eqs. (3a) and (5b). It should be noted that unlike cold-bending for open sections, the elastic springback for cold-formed SHS does not fully unload the bending moment M_{bend} (Liu *et al.* 2015). This springback moment can be defined as

$$M_{springback} = \varphi M_{bend} \tag{13}$$

where φ is a reduction factor dependent on the constraint that the corner is subjected to during the elastic springback. In this study, $\varphi = 0.9$ is used according to the 2D plane strain FE analysis result.

The final transverse stress state is the summation of the plastic stress distribution caused by bending and the unloading stress from the elastic springback

$$\sigma_\theta^{residual} = \sigma_\theta^{bend} - \sigma_\theta^{Springback} \tag{14a}$$

$$\sigma_\emptyset^{residual} = \sigma_\emptyset^{bend} - \sigma_\emptyset^{Springback} \tag{14b}$$

4. Validation of the analytical model

4.1 FE simulation

In order to verify the analytical model derived in Section 3, a 2D plane strain FE model is built to simulate the forming of residual stress in the corner of the tested cold-formed thick-walled SHS. As shown in Fig. 12(a), this model consists of 2D deformable quarter section (flat strip) and analytically rigid roller and roller die. Dense mesh is attributed to the corner area and transition mesh is set at the boundaries between the coarse and fine mesh.

Fig. 12(b) shows the Mises stress distribution of the section during bending. It can be seen from Fig. 12(b) that the neutral axis of the flat area is at the middle surface while that of the corner area is slightly shifted towards the inner surface. The stresses are generally symmetrically distributed about the neutral axis. Although large area of the corner is undergoing plastic straining, there is still a small-depth elastic core. However, this elastic core diminishes when the bending radius r_c further decreases. When the final bending profile is reached, 0.5mm displacement load (to fully unload the bending moment, 0.56 mm is needed) is applied on the boundaries to simulate the constrained springback. The final transverse and longitudinal residual stress distributions are shown in Figs. 13(a) and (b), respectively. It should be noted that the transverse residual stress (Fig. 13(a)) is not necessarily compressive on the outer surface. This amount is dependent on the amount of springback action the corner is subjected to.

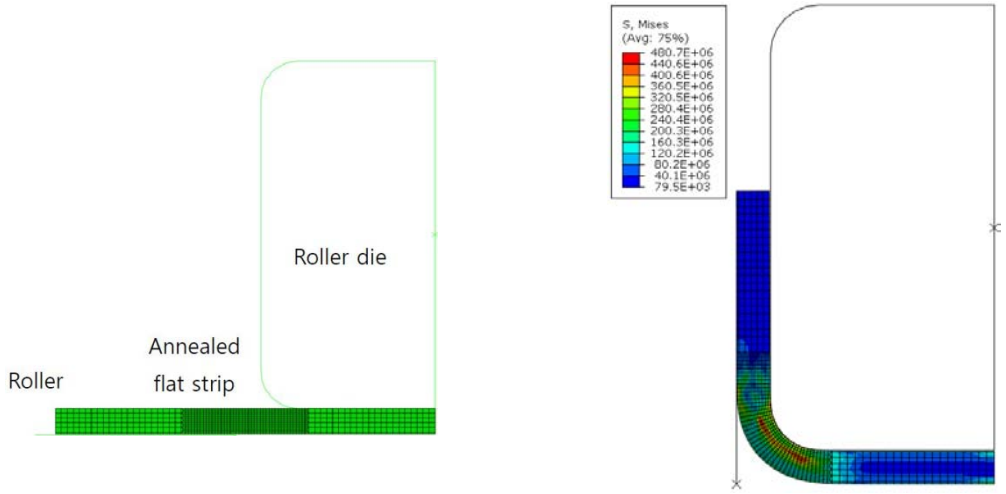

(a) FE model with mesh (b) Mises stress during bending

Fig. 12 Quarter SHS model for FE analysis

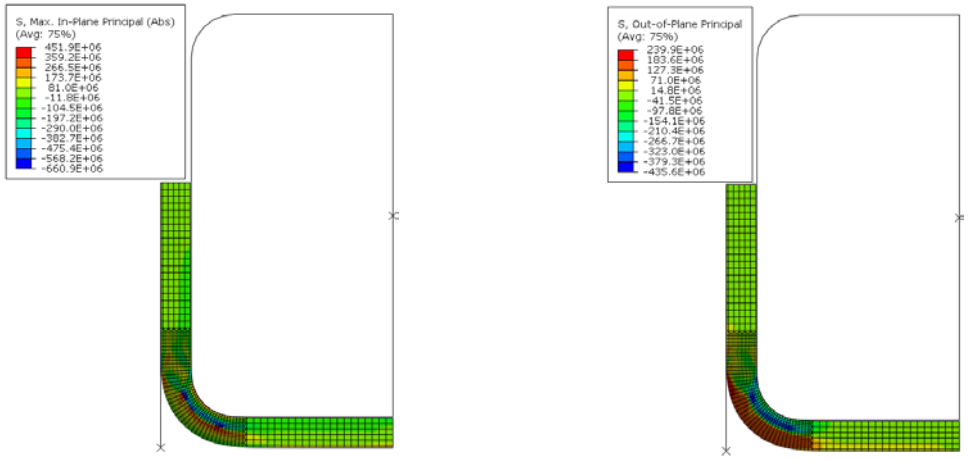

(a) Transverse residual stress (b) Longitudinal residual stress

Fig. 13 Residual stress distribution by FE analysis

4.2 Comparison between the FE and analytical model

Figs. 14(a) and (b) show the equivalent (Mises) strain and stress distribution of the corner at full bending state, respectively. It can be seen from Figs. 14(a) and (b) that the analytical model agrees reasonably well with the FE model. The differences (calculated as Analytical model/FE model×100%-100%) for the surface equivalent strains are 4.7% and -5.8% for the outer and inner surfaces, respectively, while the differences for the surface equivalent stresses are -0.56% and 5.9% for the outer and inner surfaces, respectively. The differences between the two models increase from the surfaces towards the neutral axis due to the absence of the radial stress σ_r in the analytical model. Under elastic status, σ_r is zero on the outer and inner surfaces and maximum

near the neutral axis (Eq. (3b)). As a result, the precision of the analytical model in the core is not as good as that near the outer and inner surfaces. Fig. 14c shows the final equivalent residual stress distribution. Similar to the equivalent strain and stress distribution at full bending, the equivalent residual stress distribution of the analytical model agrees well with the FE model near the surface but not good enough near the neutral axis. It should be noted that due to the absence of σ_r, the equivalent stress in the elastic core obtained by the analytical model is close to zero (Figs. 14(b) and (c)). Besides, the position of the neutral axis of the FE model is slightly lower than that of the analytical model and further away from the middle surface. The neutral axis in the analytical model is 0.7 mm (5.5% of thickness) away from the middle surface, while that in the FE model is 1.06 mm (8.3% of thickness) from the middle surface. This difference is mainly caused by the second shifting of neutral axis when plasticity takes place, which is ignored in the analytical model.

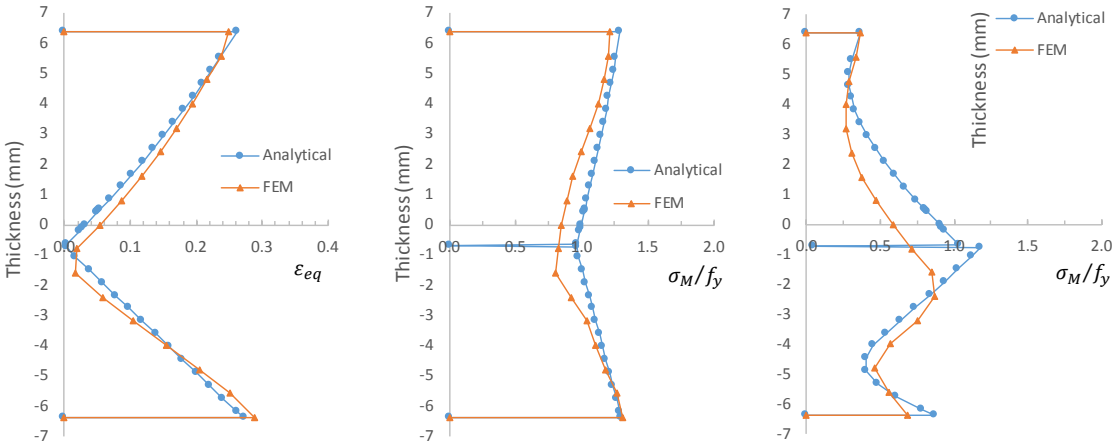

(a) Equivalent strain at full bending (b) Equivalent stress at full bending (c) Equivalent stress after springback

Fig. 14 Equivalent plastic strain and stress

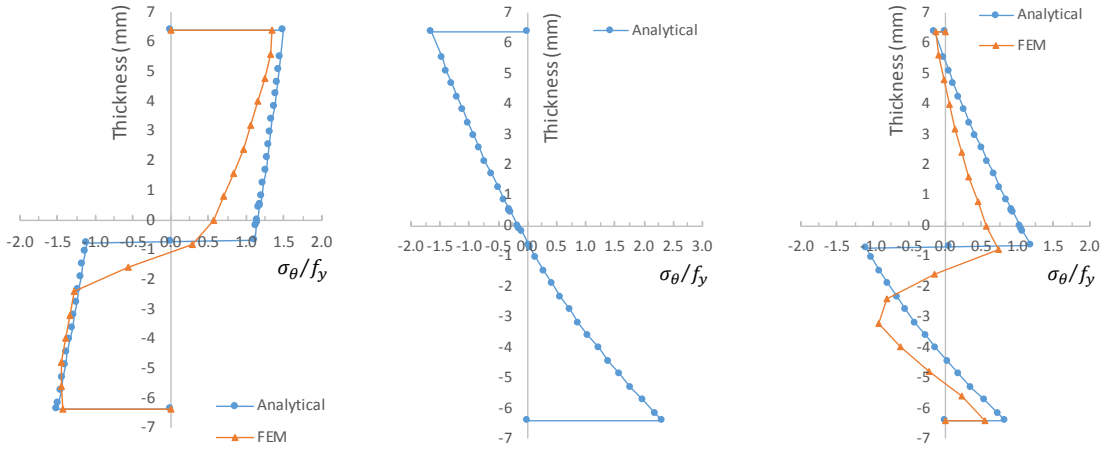

(a) Plastic bending (b) Elastic springback (c) Residual stress

Fig. 15 Self-equilibrating transverse residual stress

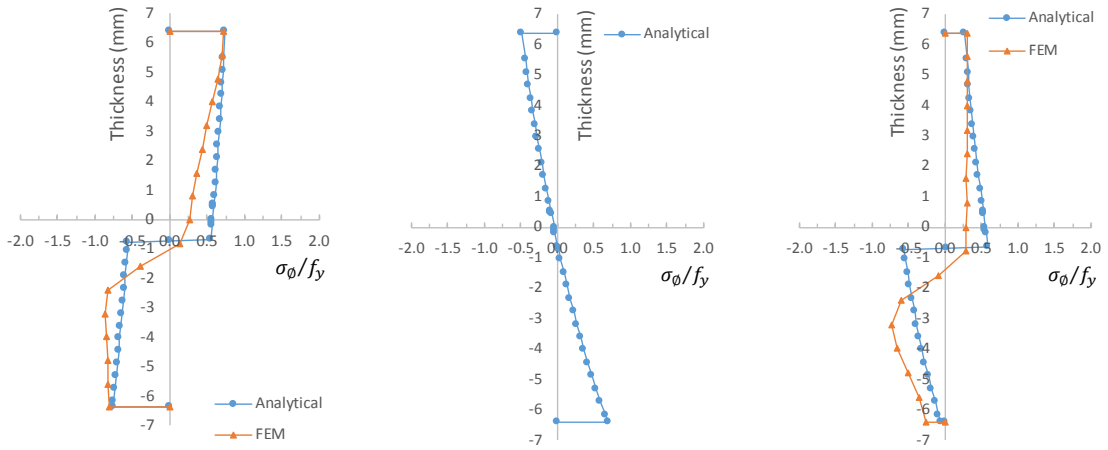

(a) Plastic bending (b) Elastic springback (c) Residual stress

Fig. 16 Self-equilibrating longitudinal residual stress

Figs. 15(a) and 16(a) show the predicted transverse and longitudinal stress distribution at full bending, respectively. The unloading elastic springback stress distributions in the transverse and longitudinal directions are show in Figs. 15(b) and 16(b), respectively, while the final transverse and longitudinal residual stress distributions are shown in Fig. 15(c) and 16(c), respectively. It can be seen from the above Figs. that all the through thickness stress distribution patterns are nonlinear and not symmetrical to the neutral axis, which is essentially different from the cold-formed thin-walled SHSs. Although the analytical model is not able to predict the stress near the neutral axis as precisely as the FE model does, the accuracy near the outer and inner surfaces are reasonably good.

4.3 Comparison between test results and the analytical model

Since the surface residual stresses can be treated as generally linearly distributed (Figs. 15(c) and 16(c)), the surface stress (AM-surface), 1mm depth stress (AM-1mm), and the mean stress of these two (AM-mean) are calculated and compared with the results by the hole-drilling test, as

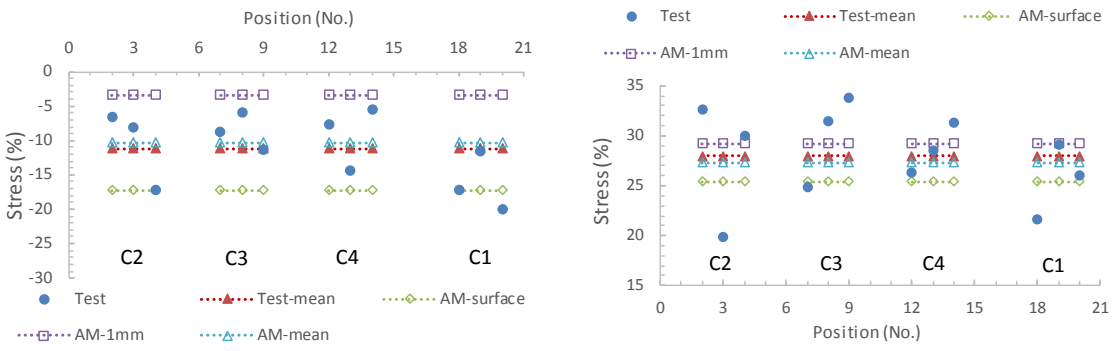

(a) transverse stress (b) longitudinal stress

Fig. 17 Comparison between test result and analytical solution

shown in Fig. 17. For the transverse residual stress, it can be seen from Fig. 17(a) that only 1 data point is outside the predicted range and the difference between the mean values of the analytical model and test is only 0.9% of the yield strength. As for the longitudinal stress distribution, the diversity is larger (Fig. 17(b)). Only half of the data points are within the predicted range (AM-surface to AM-1mm). However, the mean stresses from the test agree well with the analytical model prediction. The AM-mean is only 0.7% (of the yield strength) lower than that of the Test-mean. Therefore, it is confirmed that the proposed surface residual stress distribution model in Fig. 7(a) is valid.

5. Conclusions

The magnitude and effect of the transverse and longitudinal surface residual stresses contained in cold-formed thick-walled SHS is studied. Compared to cold-formed thin-walled SHS, the tested cold-formed thick-walled SHS contains similar magnitude of longitudinal residual stresses in the flat area but higher stress levels in the corner and welding area. Although the residual stress level in the transverse direction is much lower than that in the longitudinal direction and is less frequently studied, these stresses tend to open the section as well. In order to theoretically predict the residual stress distribution in the corners of cold-formed thick-walled SHSs, an analytical elastic-plastic large displacement model is proposed. 2D FE model is employed to simulate the forming of residual stresses in the corners due to cold bending and verify the proposed analytical model. It is shown that good agreement has been achieved for the surface residual stresses in both transverse and longitudinal directions. By analyzing the through thickness stresses, it is found out that the residual stress distribution pattern of the thick-walled SHS is totally different from that of the thin-walled SHS. It is also shown that during bending the thick-walled SHS, shifting of neutral axis must be considered, since it would lead to non-linear and non-symmetrical distribution of stresses through the thickness. Finally, the analytical model is validated by comparing the surface stress distribution prediction with the experimental results.

References

Abambres, M. and Quach, W.M. (2016), "Residual stresses in steel members: a review of available analytical expressions", *Int. J. Struct. Integrity*, **7**(1), 70-94.

AISC (2005), Specification for structural steel buldings, ANSI/AISC 306-05; Americal Institute of Steel Construction, Chicago, IL, USA.

AISI (1996), Cold-formed steel deseign manual; American Iron and Steel Institute, Washington D.C., USA.

Amouzegar, H., Schafer, B.W. and Tootkaboni, M. (2016), "An incremental numerical method for calculation of residual stresses and strains in cold-formed steel members", *Thin-Wall. Struct.*, **106**, 61-74.

ASTM (2008), ASTM E837-08: Standard test method for determining residual stresses by the hole-drilling strain gauge method; ASTM International, West Conshohocken, PA, USA.

BSI (1999), BS EN 2566-1: Steel - Conversion of elongation values - Part 1: Carbon and low alloy steels, British Standards Institution, London, UK.

BSI (2001), BS EN 10002-1: tensile testing of metallic materials: part1 method of test at ambient temperature. London, British Standards Institution.

BSI (2005), Eurocode 3: design of steel structures: part 1-1 general rules and rules for buildings, BS EN 1993-1-1, British Standard Institution, London, UK.

BSI (2006), BS EN 10219: cold formed welded structural hollow sections of non-alloy and fine grain steels,

part 1: Technical delivery conditions, British Standards Institution, London, UK.
Gardener, L., Saari, N. and Wang, F. (2010), "Comparative experimental study of hot-rolled and cold-formed rectangular hollow sections", *Thin-Wall. Struct.*, **48**(7), 495-507.
Jandera, M. and Machacek, J. (2014), "Residual stress influence on material properties and column behaviour of stainless steel SHS", *Thin-Wall. Struct.*, **83**, 12-18.
Key, P.W. and Hancock, G.J. (1993), "A theoretical investigation of the column behaviour of cold-formed square hollow sections", *Thin-Wall. Struct.*, **16**(1-4), 31-64.
Li, S.H., Zeng, G., Ma, Y.F., Guo, Y.J. and Lai, X.M. (2009), "Residual stresses in roll-formed square hollow sections", *Thin-Wall. Struct.*, **47**(5), 505-513.
Liu, T., Wang, Y., Wu, J., Xia, X., Wang, J., Wang, W. and Wang, S. (2015), "Springback analysis of Z & T-section 2196-T8511 and 2099-T83 Al–Li alloys extrusions in displacement controlled cold stretch bending", *J. Mater. Process. Technol.*, **225**, 295-309.
Ma, J.L., Chan, T.M. and Young, B. (2015), "Material properties and residual stresses of cold-formed high strength steel hollow sections", *J. Construct. Steel Res.*, **109**, 152-165.
Mashiri, F.R., Paradowska, A., Uy, B., Tao, Z., Khan, M. and Dayal, P. (2014), "Residual stresses distribution measured by neutron diffraction in fabricated square high strength steel tubes", *Proceedings of the 7th International Conference on Mechanical Stress Evaluation by Neutrons and Synchrotron Radiation, MECA SENS 2013*, Sydney, NSW, Australia, September.
Massonnet, C., Olszak, W. and Phillips, A. (1979), *Plasticity in Structural Engineering Fundamentals and Applications*, Springer-Verlag Wien, New York, NY, USA.
Moen, C.D., Igusa, T. and Schafer, B.W. (2008), "Prediction of residual stresses and strains in cold-formed steel members", *Thin-Wall. Struct.*, **46**(11), 1274-1289.
Quach, W.M., Teng, J.G. and Chung, K.F. (2004), "Residual stresses in steel sheets due to coiling and uncoiling: a closed-form analytical solution", *Eng. Struct.*, **26**(9), 1249-1259.
Spoorenberg, R.C., Snijder, H.H. and Hoenderkamp, J.C.D. (2010), "Experimental investigation of residual stresses in roller bent wide flange steel sections", *J. Construct. Steel Res.*, **66**(6), 737-747.
Timoshenko, S. and Goodier, J.N. (1970), *Theory of Elasticity*, McGraw-Hill, New York, NY, USA.
Tong, L., Hou, G., Chen, Y., Zhou, F., Shen, K. and Yang, A. (2012), "Experimental investigation on longitudinal residual stresses for cold-formed thick-walled square hollow sections", *J. Construct. Steel Res.*, **73**, 105-116.
Wang, Y.B., Li, G.Q. and Chen, S.W. (2012), "The assessment of residual stresses in welded high strength steel box sections", *J. Construct. Steel Res.*, **76**, 93-99.
Weng, C. and White, R. (1990), "Cold-bending of thick high-strength steel plates", *J. Struct. Eng.*, **116**(1), 1(40), 40-54.
Withers, P.J., Turski, M., Edwards, L., Bouchard, P.J. and Buttle, D.J. (2008), "Recent advances in residual stress measurement", *Int. J. Press. Vessel. Pip.*, **85**(3), 118-127.
Yu, T.X. and Zhang, L.C. (1996), *Plastic Bending: Theory and Applications*, World Scientific Publishing Co., NY, USA.
Zhu, H.X. (2007), "Large deformation pure bending of an elastic plastic power-law-hardening wide plate: Analysis and application", *Int. J. Mech. Sci.*, **49**(4), 500-514.

BU